Structural, magneto-electronic and thermophysical properties of the new d^0 quaternary heusler compounds KSrCZ (Z =P, As, Sb)

A. Taleb[a,*], A. Chahed[a], M. Boukli[a], H. Rozale[a], B. Amrani[a], M. Rahmoune[a] and A. Sayede[b]
[a] *Condensed Matter and Sustainable Development Laboratory (LMCDD), University of Sidi Bel-Abbes, Sidi Bel-Abbes 22000, Algeria.*
[*] *e-mail : talebaek83@gmail.com*
[b] *UCCS, CNRS-UMR 8181, Université d'Artois, Faculté des Sciences Jean Perrin, Rue Jean Souvraz, SP 18, 62307 Lens Cedex, France.*

Received 5 December 2019; accepted 25 February 2020

Investigation of band structure and the thermo-physical response of the d^0 new quaternary Heusler compounds KSrCZ (Z = P, As, Sb) within the framework of density functional theory with full-potential linearized augmented plane wave method has been analyzed. Results showed that $type - Y3$ is the most favorable atomic arrangement. All the compounds are found to be half-metallic ferromagnetic materials with an integer magnetic moment of 2.00 μB and a half-metallic gap E_{HM} of 0.292, 0.234, and 0.351 eV, respectively. The half-metallicity of KSrCZ (Z = P, As, Sb) compounds can be kept in a quite large hydrostatic strain. Thermoelectric properties of the KSrCZ (Z = P, As, Sb) materials are additionally computed over an extensive variety of temperatures, and it is discovered that all compounds demonstrate a higher figure of merit. The properties of half-metallicity and higher Seebeck coefficient make these materials a promising candidates for thermoelectric and spintronic device applications.

Keywords: Quaternary heusler compounds; electronic structures; magnetic properties; thermoelectric properties.

PACS: 63.20.Dj; 71.15.Mb; 62.50.+p; 72.15.Jf; 71.20.Be

DOI: https://doi.org/10.31349/RevMexFis.66.265

1. Introduction

In recent decades, quaternary Heusler alloys have attracted much interest due to their excellent properties such as high spin-polarization and half-metallic ferromagnetism (HMF), where they have possible uses in spintronic and thermoelectric applications [1-4]. The latest trend is towards looking for new sp or d^0 HM compounds, and some studies reveal that the materials without transition metal elements, d^0 compounds, would be a new type of HM materials where the spin polarization and magnetic order are mainly from the anion p-electrons of anions [5-7]. Many works on d^0 compound with ternary half-Heusler structure and full-Heusler structure have been done theoretically [8-12]. However, research and report on d^0 HM compounds with quaternary Heusler structure are still rare [13-17].

Compared with the traditional HMF quaternary Heusler with transition metal elements having large stray fields, these d^0 materials are more meaningful in real applications because of the smaller magnetic moments. Also the thermoelectric (TE) [1-4] quaternary Heusler materials are regarded as the alternate sources of energy due to their ability to convert waste heat into electricity and they have used for power generation because they are cheaper, abundant in nature, and environmentally friendly, *i.e.*, free from toxic elements. To the best of our knowledge, no study on our d^0 compounds KSrCZ (Z = P, As, Sb) with quaternary Heusler structure has been reported in the literature. The characteristics of energy bands and the origin of the half-metallic gap were not studied. The effect of volumetric on the half-metallicity character was not investigated. The thermoelectric performances such as Seebeck coefficient, electrical and thermal conductivity, and thermopower factor are no calculated. In this paper, the structural, electronic, magnetic, and thermoelectric properties of new quaternary d^0 Heusler compounds KSrCZ (Z = P, As, Sb) have been studied by using the first-principles calculations. We have chosen this series of compounds with the hope that they would exhibit half-metallicity, good magnetic and thermoelectric properties. Our paper is organized as follows. The theoretical background is presented in Sec. 2. Results and discussion are presented in Sec. 3. A summary of the results is given in Sec. 4.

2. Computational method

The calculations were performed within the density functional theory (DFT) [18]. We use the full potential linear-augmented-plane waves the plus local orbital (FP-LAPW) method [19] implemented in the Wien2k package [20]. The exchange-correlation potential was treated under the generalized gradient approximation (GGA) [21]. The partial waves used inside the atomic spheres are expanded up to $l_{\max} = 10$ with a matrix size RmtKmax equal to 8. A $20 \times 20 \times 20$ k-point mesh was used as a base for the in the first Brillouin zone was found to be sufficient in most cases. Within the (FP-LAPW) method, we impose a convergence criterion of 10^{-5} in the total energy to improve accuracy in the spin-polarized calculations.

3. Results and discussion

In general, the quaternary Heusler compounds are compounds adopted in LiMgPdSn-type crystal structure denoted

TABLE I. Calculated total energies E_{tot} (in Ry) per formula unit, equilibrium lattice constant a_0 (in Å), the bulk modulus B (in GPa) for KSrCZ (Z= P, As, Sb) compounds in theirs different structures type and magnetic configurations.

Compound	structure	E_{tot} (Ry)		a_0 (Å)	B_0 (GPa)
		NM	FM	FM	FM
KSrCP	$Type-Y1$	-8324.009601	-8324.009398	7.0471	38.0318
	$Type-Y2$	-8324.089225	-8324.102824	7.3131	32.7388
	$Type-Y3$	-8324.098220	-8324.112673	7.3218	32.5218
KSrCAs	$Type-Y1$	-12162.030023	-12162.029921	7.1744	35.6927
	$Type-Y2$	-12162.098230	-12162.099959	7.4516	29.8852
	$Type-Y3$	-12162.098405	-12162.109866	7.4775	29.8643
KSrCSb	$Type-Y1$	-20607.103600	-20607.103042	7.4618	31.25
	$Type-Y2$	-20607.153885	-20607.16728	7.8367	28.1845
	$Type-Y3$	-20607.153835	-20607.191886	7.8267	25.158

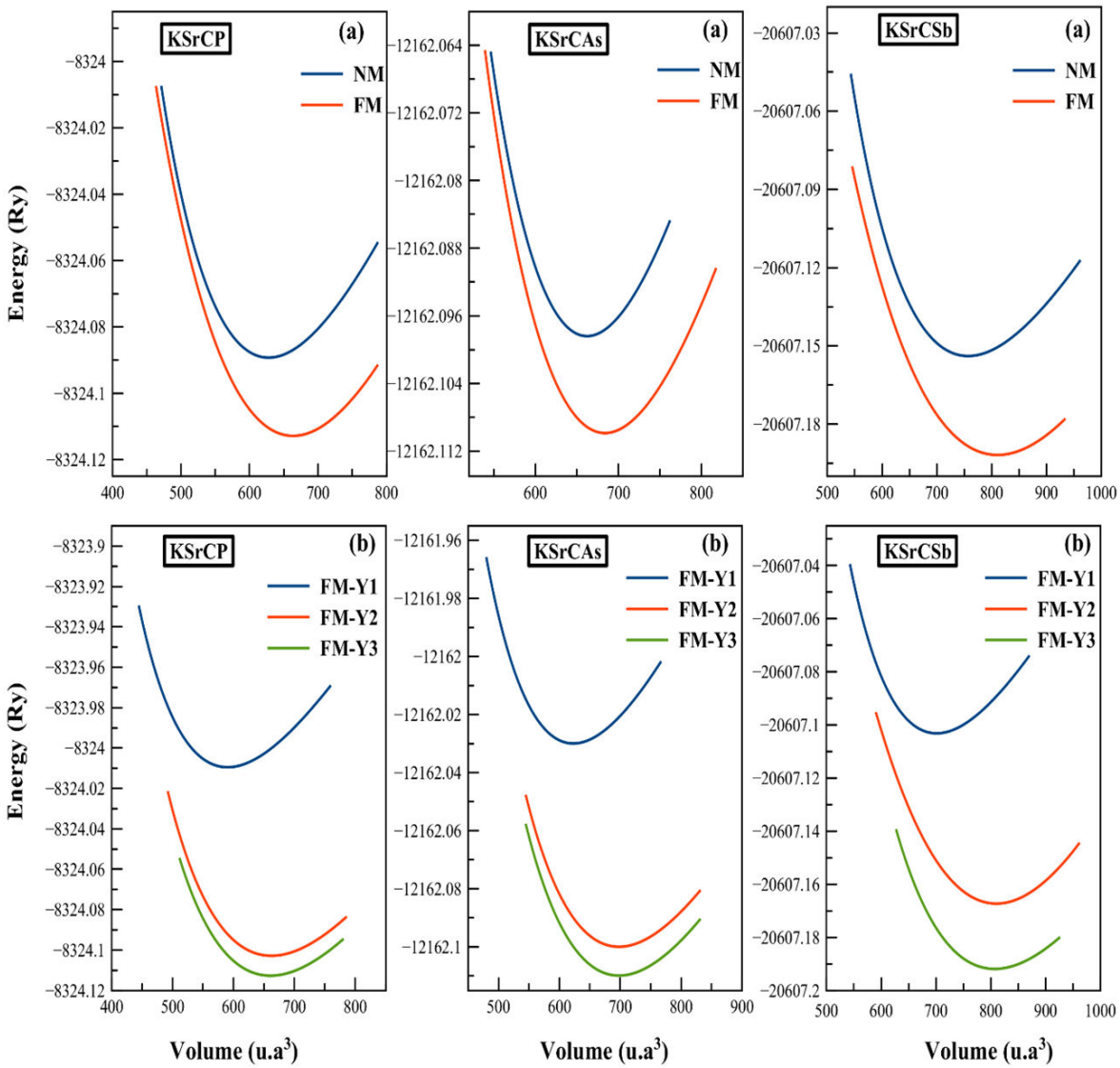

FIGURE 1. Total energy as a function of volume per formula unit (f.u.) in the magnetic states $FM-Y3$ and $NM-Y3(a)$ and the three atomic arrangements type $FM-Y1$, $FM-Y2$ and $FM-Y3$(b) for the KSrCZ (Z = P, As, Sb) compounds.

as Y (space group 216) [22]. There are three possible different types of atom arrangement in the quaternary Heusler compound XX'YZ: Y1: X (0, 0, 0), X' (0.25, 0.25, 0.25), Y (0.5, 0.5, 0.5), and Z (0.75, 0.75, 0.75); Y2: X (0, 0, 0), X'(0.5, 0.5, 0.5), Y (0.25, 0.25, 0.25), and Z (0.75, 0.75, 0.75); Y3: X (0.5, 0.5, 0.5), X' (0, 0, 0), Y (0.25, 0.25, 02.5), and Z (0.75, 0.75, 0.75). To confirm the structural and magnetic ground states of $Y1$, $Y2$ and $Y3$ configuration, the total energies of the non-magnetic (NM) and ferromagnetic (FM) states as a function of the lattice constant of the three compounds were calculated and the obtained curves are shown in Fig. 1. The results show that the energies of $FM-Y3$ state are lower, indicating that $FM-Y3$ state is the ground state among three magnetic states. In Table I, we report our calculated equilibrium lattice constant a_0, along with the bulk modulus B_0, and the total energy Etot in their different structural and magnetic configurations. As shown in Table I, the obtained equilibrium lattice constant increases with the increase of the atomic radius of anion: 7.3218, 7.4775, and 7.8267Å for KSrCP, KSrCAs, and KSrCSb, respectively. Also, the highest calculated bulk moduli for KSrCZ (Z =P, As, Sb) compounds in *FM-Y3* configuration confirm the stability of this structure. Based on this, all the further calculations on electronic, magnetic, and thermoelectric properties of KSrCZ (Z = P, As, Sb) were performed on this structure only, *i.e*, in the type *FM-Y3* structure.

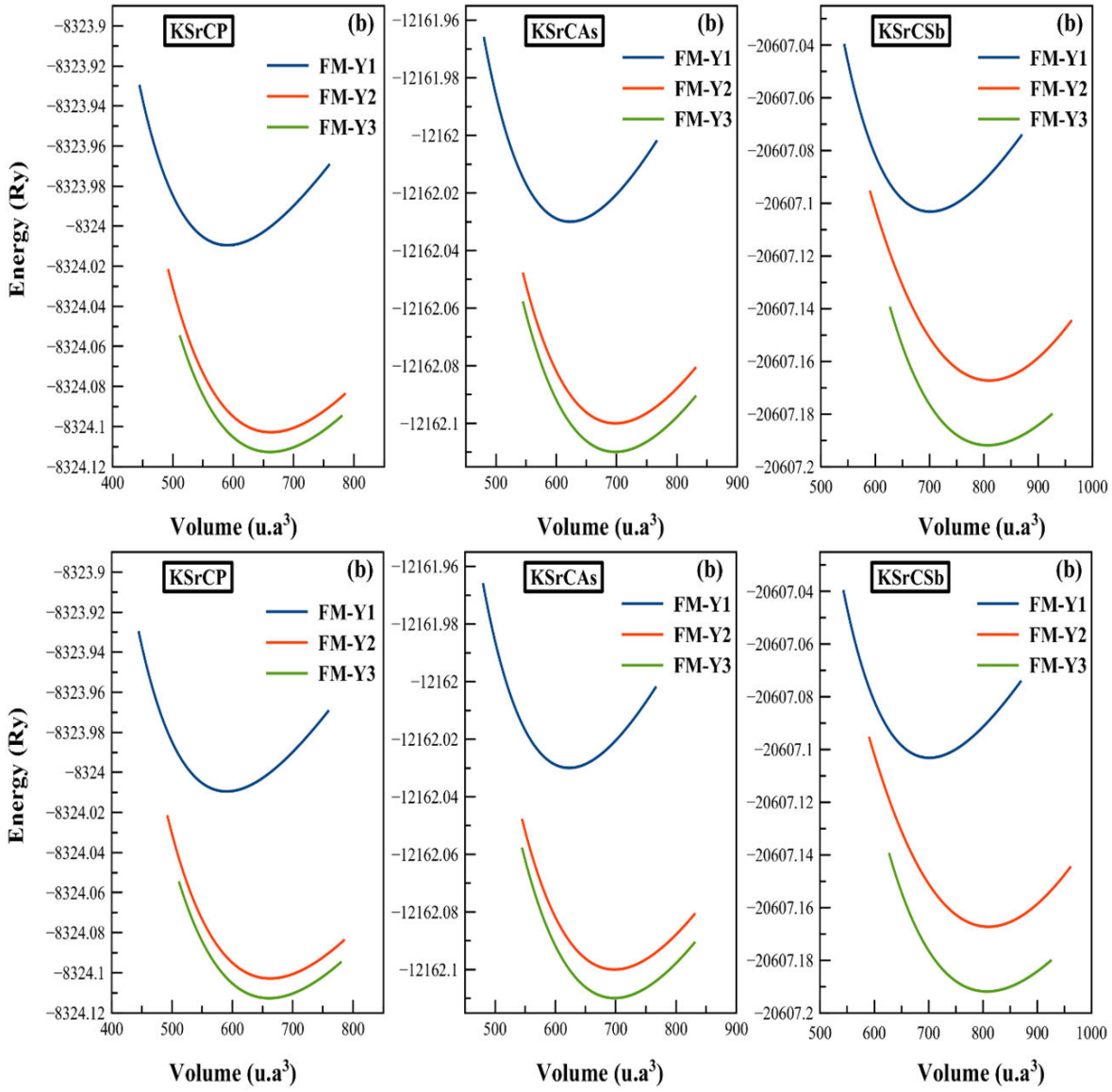

FIGURE 2. Spin-polarized band structure for the KSrCZ (Z = P, As, Sb) compounds at their equilibrium lattice constant.

TABLE II. The semiconducting gap E_g (in eV), the half-metallic gap E_{HM} (in eV), total magnetic moment μ_{tot} (in μ_B), the magnetic moment per atom (K, Sr, C, P, As, Sb), and magnetic moment in the interstitial region μ_{int} in compounds KSrCZ (Z= P, As, Sb).

Compound	E_g	E_{HM}	μ_{tot}	μ_K	μ_{Sr}	μ_C	μ_Z	μ_{int}
KSrCP	0.87	0.292	2	0.018	0.03	1.622	-0.03	0.36
KSrCAs	0.80 0.234	2	0.016	0.028	1.61	-0.024	0.37	
KSrCSb	0.92	0.351	2	0.01	0.02	1.618	-0.028	0.38

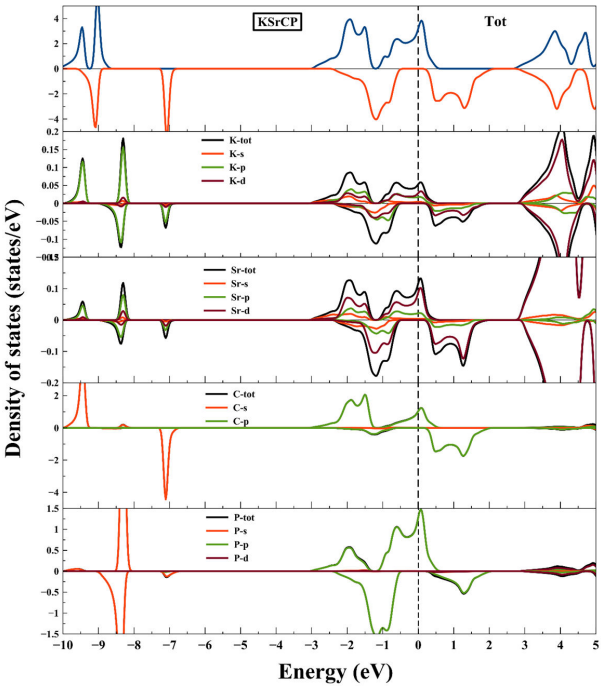

FIGURE 3. Spin-polarized total and partial densities of states (DOS) for the KSrCP compound.

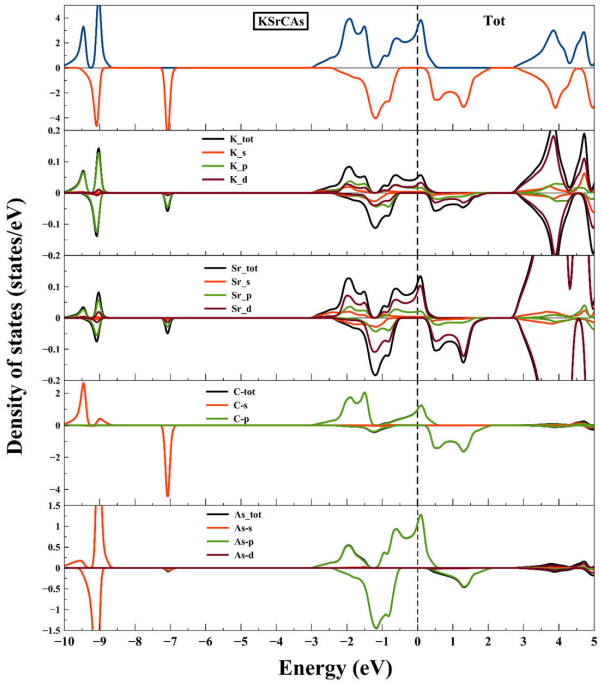

FIGURE 4. Spin-polarized total and partial densities of states (DOS) for the KSrCAs compound.

The calculated band structures of KSrCZ (Z =P, As, Sb) compounds with *FM-Y3* type configuration at equilibrium lattice constants have been illustrated in Fig. 2. The spin-up triplet band crosses the Fermi level and exhibits a metallic behavior while the spin-down band are semiconducting with a forbidden indirect band gaps E_g (W-Δ) around the Fermi level confirming that these compounds are half-metallic (HM) with 100% spin polarization. The predicted half-metallic gaps E_{HM} are listed in Table II. This gap is known to be essential to describe the stability of HM magnetism of a half-metal [23]. As shown in Table II, KSrCP, KSrCAs, and KSrCSb display large HM gaps of 0.292, 0.234, and 0.351 eV, respectively, illustrating stable HM features. Unfortunately, no experimental measurements and theoretical data band gaps E_g and E_{HM} for the investigated compounds are carried for comparison.

To understand the electronic structure further, the calculated total and partial density of states (DOS) for these compounds are presented in Figs. 6-8. It can be seen that the DOS of all compounds have a similar structure. From partial DOS, it is clear that the spin-up triplet state across the Fermi level is mainly from $C-p$ states with smaller contribution coming from the $P-$, $As-$, and $Sb-p$ states. For the spin-down states of these materials, the top of the valence bands is mainly from the $As-p$ states, while the bottom of the conduction bands is mainly from the $C-p$ states responsible for gap formation. Our total magnetic moment μ_{tot} per formula unit calculated is found to be integer values 2.00 μB for all compounds. This integer value is also a typical HM characteristic. We also list in Table II the local magnetic moments at the K, Sr, C, and Z (Z= P, As, Sb) sites. As seen in Table II, for all three half-metal compounds, the main contribution to the total magnetic moment is from p states of C.

Because the half-metallic materials are usually prepared as thin films for spintronic applications, where the lattice constant of the half-metallic material strongly depends on the substrate lattice parameter and correspondingly the half-metallicity may be destroyed. Fig. 4 shows the total magnetic moments with respect to the different lattice constants. The magnetic moments remain integral 2 μB until the lattice is compressed to a critical value of 6.91, 7.17, and 7.38 Å for KSrCZ (Z = P, As, Sb), respectively. This

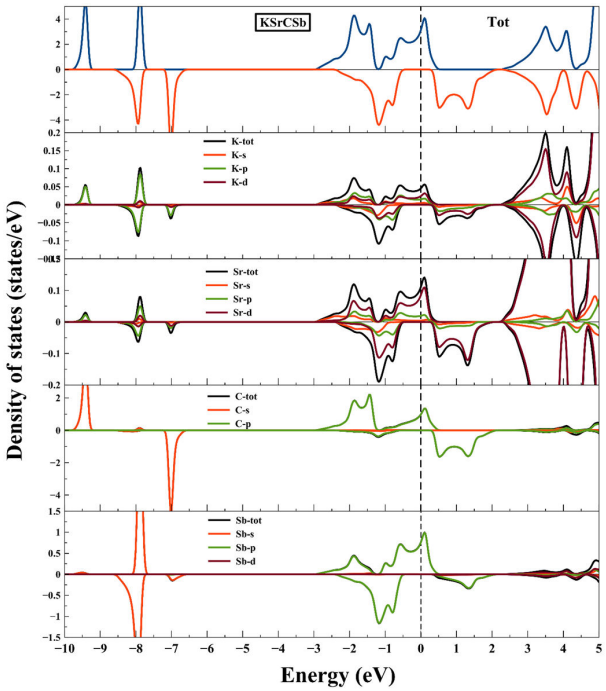

FIGURE 5. Spin-polarized total and partial densities of states (DOS) for the KSrCSb compound.

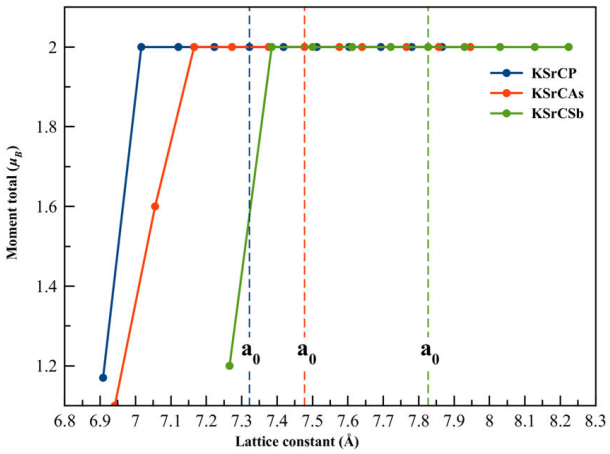

FIGURE 6. The total magnetic moments for KSrCZ (Z = P, As, Sb) as a function of the lattice constants.

indicates that the half-metallicity is preserved up to a lattice contraction of 4.18%, 4.17%, and 5.65% for all three quaternary Heusler compounds, reflecting the order of magnitude of half-metallic gap EHM. On the other hand, it is found that KSrCSb is the most stable compared to KSrCP and KSrCAs.

Thermoelectric (TE) materials transform the waste heat energy into usable electric energy, and thereby offer a possible solution to the present-day energy crisis. This category of materials is currently being investigated at faster rates than the other technologically important materials because of their eco-friendly and efficient energy management [24]. For the first time, the thermoelectric properties of KSrCZ (X = P, As, Sb) compounds are calculated by the BoltzTrap code [25].

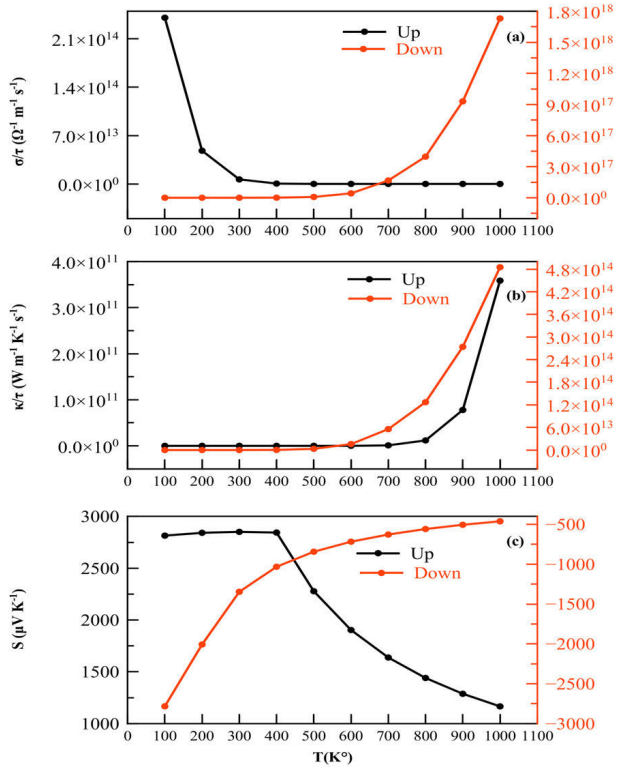

FIGURE 7. The variation of electrical conductivity σ/τ (a), thermal conductivity κ/τ (b) and Seebeck coefficient S (c) versus temperature in both the spin states for KSrCP.

In this study, we calculated the electrical conductivity σ/τ, thermal conductivity κ/τ, Seebeck coefficient S, and figure of merit ZT. An efficient thermoelectric material is required to have high electrical conductivity, low thermal conductivity, and a large Seebeck coefficient.

The temperature variation of electrical conductivity (σ/τ) is reported in Figs. 7-9(a). We observe that the electrical conductivity of three of these compounds decreases in the spin-up state, which confirms the metallic behavior in the spin-up state. While electrical conductivity increases with the increase in temperature, which again confirms the semiconducting behavior in the spin-down state and thus supports the band structure. The Electronic part of the thermal conductivity κ/τ shows a negligible variation up to 600 K and an exponential increase at higher temperatures, as depicted in Figs. 7-9(b). The Seebeck coef-

TABLE III. Values of electrical conductivity σ/τ (in $10^{13}\Omega^{-1}\text{m}^{-1}\text{s}^{-1}$), thermal conductivity κ/τ (in 10^{9} W $\text{m}^{-1}\text{K}^{-1}\text{s}^{-1}$) and Seebeck coefficient S (in μV K^{-1}), and figure of merit ZT at 300 K for KSrCZ (Z= P, As, Sb) compounds.

Compound	σ/τ	κ/τ	S	ZT
KSrCP	1.18	6.71	-2007	0.96
KSrCAs	1.12	6.51	-1336	0.93
KSrCSb	0.16	1.23	-1567	0.95

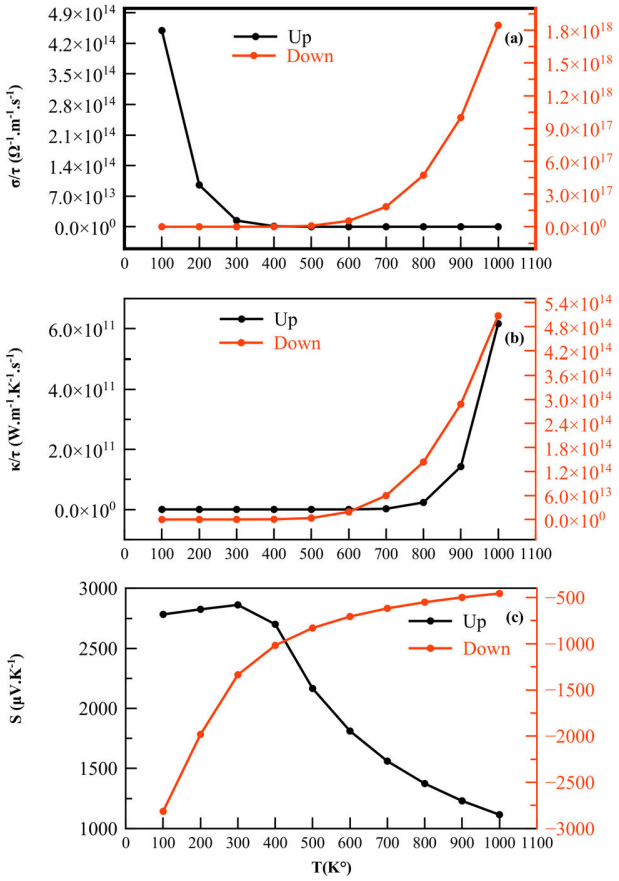

FIGURE 8. The variation of electrical conductivity σ/τ (a), thermal conductivity κ/τ (b) and Seebeck coefficient S (c) versus temperature in both the spin states for KSrCAs.

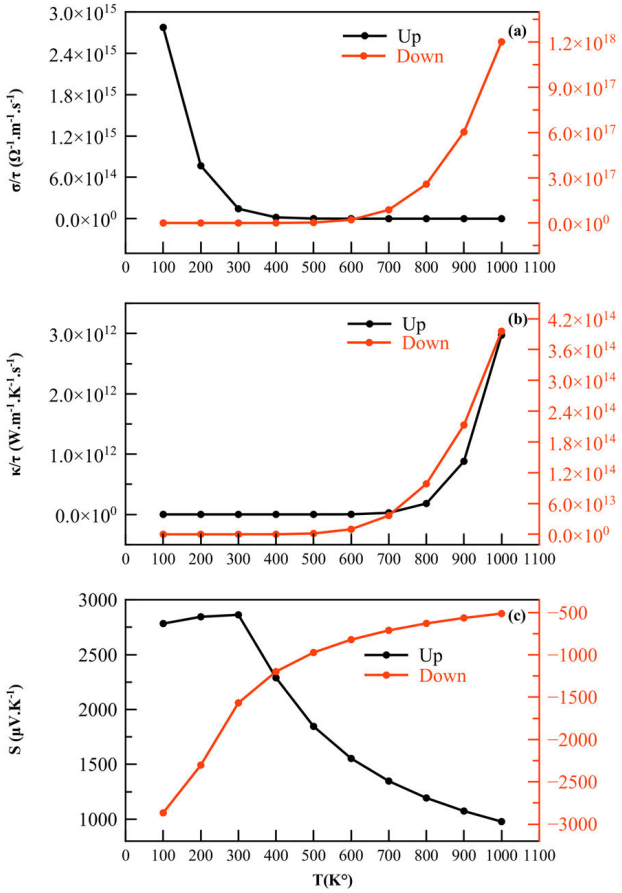

FIGURE 9. The variation of electrical conductivity σ/τ (a), thermal conductivity κ/τ (b) and Seebeck coefficient S (c) versus temperature plots in both the spin states for KSrCSb.

ficients for KSrCZ (Z = P, As, Sb) compounds are displayed as a function of temperature in Figs. 7-9(c). The observed value of the Seebeck coefficient for all compounds are positive in the spin-up channel, signifying the presence of holes as charge carriers ($p-type$), while the in spin-down channel, the negative value of S suggests electrons as charge carriers ($n-type$).

The variation of the total electrical conductivity σ/τ as a function of the temperature is plotted in Fig. 10(a). With the increase of temperature, σ/τ increases monotonously from a very small value until 500 K and beyond this temperature σ/τ increases linearly, and at 1000 K attains a value of 1.73×10^{18}, 1.85×10^{18} and 1.21×10^{18} $\Omega^{-1}\mathrm{m}^{-1}\mathrm{s}^{-1}$ for KSrCP, KSrCAs, KSrCSb, respectively. This increase could be justified by the fact that increasing temperature enhances the thermal energy of the electrons to freely form a high conducting state.

Figure 10(b) displays the temperature dependences of total thermal conductivity κ/τ. The κ/τ plots follow a similar trend as those of electrical conductivity σ/τ. The κ/τ value increases gradually, from nearly zero for all four materials in the range temperature between 100 K and 500 K. Beyond this temperature there is almost a linear increase in the range studied. The rise of the thermal conductivity with the increasing temperature is mainly due to the higher charge carrier concentration. Note in passing that the nearly indistinguishable plots (Fig. 2) suggest that KSrCZ (X = P, As, Sb) should have approximately the same band gaps (0.87, 0.8, 0.92 eV, respectively).

We also computed the total Seebeck coefficient S variation calculated by a two-current model [26] to designate its nature, as shown in Fig. 10(c). As one can see, the Seebeck coefficient of the all KSrCZ (X = P, As, Sb) Heusler compounds is negative for the entire temperature range and this negative sign of S explains that the electrons are dominant charge carriers, which in turn states that the spin-down state is dominant. Therefore, the KSrCZ (X = P, As, Sb) are n-type materials. The sharp increase in the S value at lower temperatures (< 200 K) indicates the presence of a low carrier concentration. In the range of temperature (200-1000 K), we see a slight linear decrease of the absolute value S, and at 1000 K attains a value of -461.41, -455.36 and -508.22 μV K^{-1} for KSrCP, KSrCAs, KSrCSb, respectively.

Finally, the calculated transport coefficients are now used to estimate the thermoelectric efficiency through the figure of merit ZT measurement given by the relation $ZT = (S^2\sigma\mathrm{T}/\kappa)$ and shown in Fig. 10(b). The material is consi-

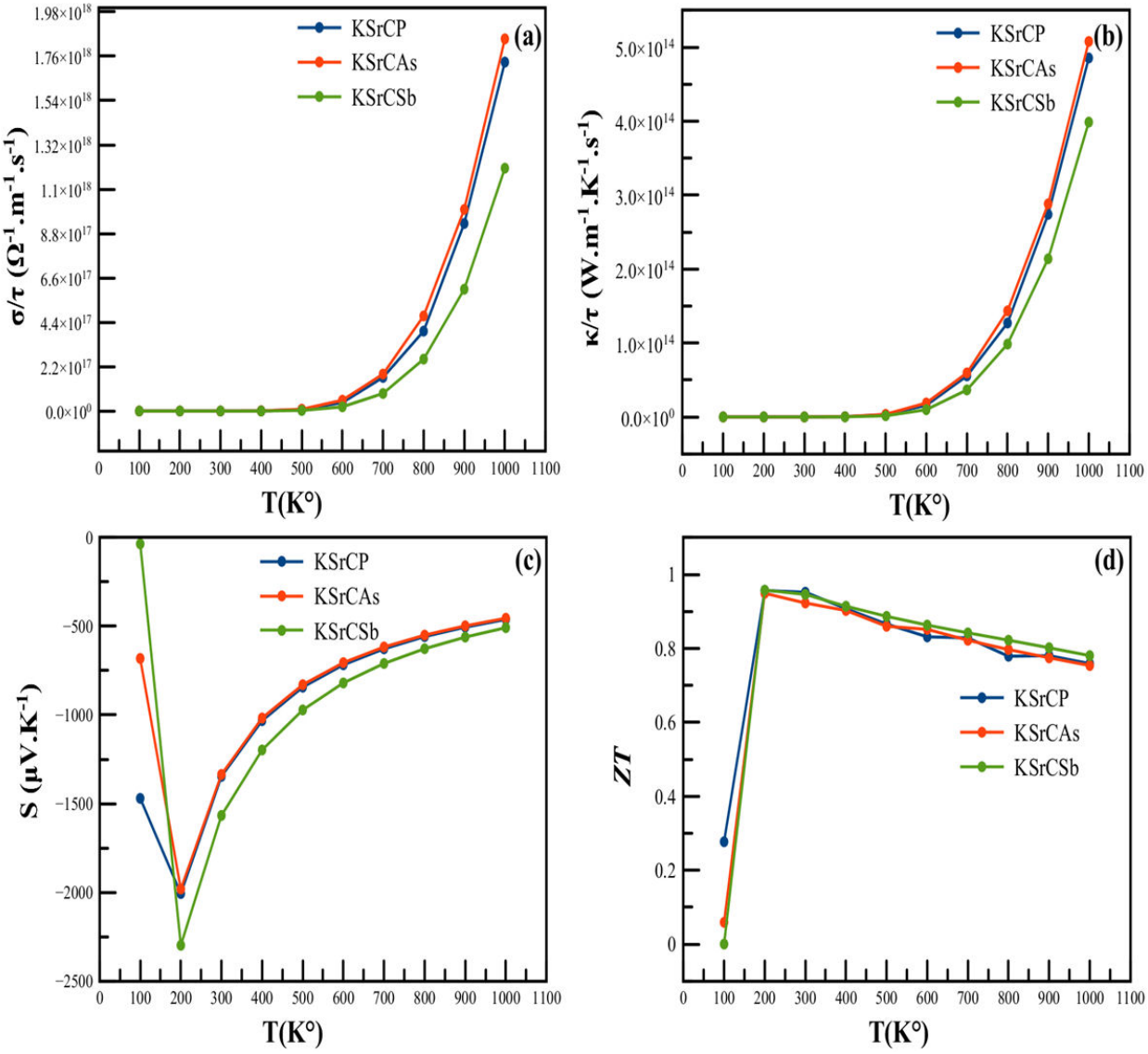

FIGURE 10. The variation of total electrical conductivity σ/τ (a), total thermal conductivity κ/τ (b), total Seebeck coefficient S (c) and figure of merit ZT (d) as a function of temperature for KSrCZ (Z = P, As, Sb).

dered as a good element for thermoelectric devices if his ZT is about or greater than unity [27]. From Fig. 10(d) the calculated value of ZT is negligible up to 100 K but, it abruptly increases to a maximum high value of 0.957, 0.96, 0.957 at 200 K for KSrCP, KSrCAs, KSrCSb, respectively corresponding to the maximum of the Seebeck coefficient S (see Fig. 10(c)). High values of the figure of merit suggest the good thermoelectric performance of these quaternary Heusler compounds, indicating they could be promising materials for applications in thermoelectric generators. The value of electrical conductivity, thermal conductivity, Seebeck coefficient, and figure of merit ZT at room temperature are summarized in Table III. These materials show higher efficiency for thermoelectric relatively in comparison for the other quaternary Heusler compounds, including transition metals [1,28-30].

4. Conclusion

In conclusion, the electronic structure, magnetic, and thermoelectric properties of the quaternary Heusler alloys KSrCZ (Z = P, As, Sb) have been calculated using the first principles full-potential linearized augmented plane waves method within the generalized gradient approximation (GGA). In all compounds, the stable type $FM + Y3$ configuration structure was energetically more favorable. At the equilibrium lattice constant, our GGA calculations show that all compounds KSrCZ (Z = P, As, Sb) are half-metallic ferromagnets (HMFs) with a large half-metallic gap E_{HM}. The half-metallicity is found to be robust to the lattice compression. Further, the transport properties of the material reveal some fruitful results. These materials exhibit high val-

ues of Seebeck coefficient and figure of merit with the room temperature values. Since these materials offer high spin-polarization, robust half-metallicity and high Seebeck coefficient make it credible applicants for spintronic and thermoelectric applications. Most of the investigated properties are reported for the first time and provide the reference for future experimental work.

Acknowledgments

This work has been supported by the PRFU project (N° B00L02UN220120190013) of the Ministry of Higher Education and Scientific Research and the Directory General of Scientific Research and Technological Development (DGRST). The authors express their appreciation and gratitude for their continuous support in this research.

1. T. M. Bhat and D. C. Gupta, *J. Magn. Magn. Mater.*, **449** (2018) 493. https://doi.org/10.1016/j.jmmm.2017.10.081
2. S. Chatterjeea *et al.*, *J. Magn. Magn. Mater.*, **478** (2019) 155. https://doi.org/10.1016/j.jmmm.2019.01.100
3. H. Karaa, M.U. Kahaly, and K. Ozdogan, *J. Alloys Compd.*, **735** (2018) 950e958. https://doi.org/10.1016/j.jallcom.201711.022
4. M.A. Hossain, M. T. Rahman, M. Khatun, and E. Haque, *Computat. Condens. Matter,* **15** (2018) 31. https://doi.org/10.1016/j.cocom.2018.03.006
5. H. Benaissa, S. Benatmane, S. Amari, and K. O. Obodo, *Spin,* **8** (2018) 1850008. https://doi.org/10.1142/S20132471850008X
6. K. L. Yao, J. L. Jiang, Z. L. Liu and G. Y. Gao, *Phys. Lett. A*, **359** (2006) 326. https://doi.org/10.1016/j.physleta.2006.06.052
7. O. Volnianska, and P. Boguslawski, *J. Phys.: Condens. Matter*, **22** (2010) 073202. https://doi.org/10.1088/0953-8984/22/7/073202
8. J. Chen, G. Y. Gao, K. L. Yao, and M. H. Song, *J. Alloys Compd.*, **509** (2011) 10172. https://doi.org/10.1016/j.jallcom.2011.08.083
9. X. P. Wei, Y. D. Chu, X. W. Sun, J. B. Deng and Y. Z. Xing, *Superlattice Microstruct.*, **74** (2014) 70. https://doi.org/10.1016/j.spmi.2014.06.018
10. H. Rozale, A. Lakdja, A. Amar, A. Chahed, and O. Benhelal, *Comput. Mater. Sci.*, **69** (2013) 229. https://doi.org/10.1016/j.commatsci.2012.12.002
11. L. Zhang, X. T. Wang, H. Rozale, J. W. Lu, and L. Y. Wang, *J. Supecond. Nov. Magn.*, **28** (2015) 3701. https://doi.org/10.1007/s10948-015-3211-6
12. M. Ahmad, Naeemullah, G. Murtaza, R. Khenata, S. BinOmran, and A. Bouhemadou, *J. Magn. Magn. Mater.*, **377** (2015) 204.
13. J. Du, S. Dong, X. T. Wang, H. Zhao, L. Y. Wang, and L. F. Feng, *AIP Adv.*, **6** (2016) 105308. https://doi.org/10.1063/1.4966143
14. J. Du *et al.*, *J. Magn. Magn. Mater.* **428** (2017) 250. https://doi.org/10.1016/j.jmmm.2016.12.038
15. J. Du *et al.*, *Superlattices Microstruct.*, **105** (2017) 39.
16. S. Rezaei and F. Ahmadian, *J. Magn. Magn. Mater.*, **456** (2018) 78. https://doi.org/10.1016/j.jmmm.2018.02.006
17. A. Bouabça, H. Rozale, A. Amar, X. T. Wang, A. Sayade, and A. Chahed, *J. Magn. Magn. Mater.*, **419** (2016) 210. https://doi.org/10.1016/j.jmmm.2016.06.018
18. P. Hohenberg, and W. Kohn, *Phys. Rev. B*, **136** (1964) 864. https://doi.org/10.1103/PhysRev.136.B864
19. E. Wimmer, H. Krakauer, M. Weinert, and A. J. Freeman, *Phys. Rev. B*, **24** (1981) 864. https://doi.org/10.1103/PhysRevB.24.864
20. P. Blaha, K. Schwarz, G. K. H. Madsen, D. Kvasnicka, and J. Luitz, *WIEN2k, An Augmented Plane Wave Local Orbitals Program for Calculating Crystal Properties*, Technische Universität Wien (2001).
21. J. P. Perdew, S. Burke and M. Ernzerhof, *Phys. Rev. Lett.*, **77** (1996) 3865. https://doi.org/10.1103/PhysRevLett.77.3865
22. X. Dai, G. Liu, G. H. Fecher, C. Felser, Y. Li, and H. Liu, *J. Appl. Phys.*, **105** (2009) 07E901. https://doi.org/10.1063/1.3062812
23. E. şasioğlu, L. M. Sandratskii, and P. Bruno, *J. Phys.: Condens. Matter.*, **17** (2005) 995. https://doi.org/10.1088/0953-8984/17/6/017
24. S. A. Khandy, and D. C. Gupta, *J. Magn. Magn. Mater.*, **441** (2017) 166. https://doi.org/10.1016/j.jmmm.2017.05.058
25. G. K. H. Madsen, and D. J. Singh, *Phys. Commun.*, **175** (2006) 67. https://doi.org/10.1016/j.cpc.2006.03.007
26. H. J. Xiang, and D. J. Singh, *Phys. Rev. B,* **76** (2007) 195111. https://doi.org/10.1103/PhysRevB.76.195111
27. T. Takeuchi, *Mater. Trans.*, **50** (2009) 2359. https://doi.org/10.2320/matertrans.M2009143
28. S. Yousuf, and D. C. Gupta, *Mater. Sci. Eng. B*, **221** (2017) 73. https://doi.org/10.1016/j.mseb.2017.04.004
29. T. T. Lin, Q. Gao, G. D. Liu, X. F. Dai, X. M. Zhang, and H. B. Zhang, *Current Appl. Phys.*, **19** (2019) 721. https://doi.org/10.1016/j.cap.2019.03.020
30. S. Yousuf and D. C. Gupta, *J. Phys. Chem. Solids*, **112** (2018) 190. https://doi.org/10.1016/j.jallcom.2017.11.239